sciendo

POLISH MARITIME RESEARCH 4 (116) 2022 Vol. 29; pp. 145-154
10.2478/pomr-2022-0052

DYNAMIC ANALYSIS AND EXPERIMENT OF UNDERACTUATED DOUBLE-PENDULUM ANTI-SWING DEVICE FOR SHIP-MOUNTED JIB CRANES

WANG Jianli[*1,2,3]
LIU Kexin[1]
WANG Shenghai[1]
CHEN Haiquan[1]
SUN Yuqing[1]
NIU Anqi[1]
LI Haolin[3]

[1] College of Marine Engineering, Dalian Maritime University, Dalian, China
[2] College of shipping, Bohai University, Jinzhou, China
[3] Bohai Shipbuilding Heavy Industry Co. Ltd, China
* Corresponding author: *wangjianli_bohai@126.com (WANG Jianli)*

ABSTRACT

This paper proposes a three degrees of freedom parallel anti-swing method by the main and auxiliary cables to address the problems related to underactuated double-pendulum anti-swing for a ship-mounted jib crane. By analysing the dynamic coupling relationship between the swing of the hook and the payload, it seeks to establish an accurate dynamic model of the anti-swing device under the ship's rolling and pitching conditions, and discusses the influence of ship excitation, the crane state, load posture and anti-swing parameters on the in-plane and out-of-plane swing angles. The analysis shows that the primary pendulum reduces the in-plane angle by 90% and the out-of-plane angle by 80%, the in-plane angle of the secondary pendulum is reduced by 90%, and the out-of-plane angle is reduced by 80%. The reliability of the simulation data is verified through experiments.

Keywords: ship-mounted cranes, underactuated double-pendulum, dynamic simulation, anti-swing control

INTRODUCTION

Cranes play a crucial function in engineering construction. The most prevalent types of cranes are bridge cranes, gantry cranes, slewing jib cranes, and tower cranes [1]. Due to the structural properties of the slewing jib crane, it is extensively employed in offshore engineering activities for the transportation of personnel and supplies between offshore platforms and ships, pipeline laying, wind turbine installation, etc. The six degrees of freedom (i.e., roll, pitch, yaw, sway, surge, and heave) are triggered by external forces such as waves, swells, and wind in the water, which impact the ship [2]. The excitation is conveyed to the payload via the hull, the crane body, and the boom. The coupling effect of the ship's excitation and the payload's inertia causes the payload to oscillate significantly [3].

In engineering, reducing the swing of the payload is accomplished mostly by manual manipulation of the crane and the servo motor of the hoisting winch. The amount of knowledge and experience of the crane operators has a significant impact on the positioning performance and suppression of the crane's swing. For first-order and second-order ship excitation, maritime cranes can employ intelligent control methods [4-9] to decrease the swing. To modify the swing of the payload, the servo drive controller transmits the speed command and position feedback information of the auxiliary cables [4]. The PID controller is able to effectively move the trolley of the crane in a short amount of time while

compensating for fluctuations in the payload mass and cable length under various situations [5]. A parallel distributed fuzzy LQR controller is created by constructing a linear quadratic regulation sub-controller based on each linear subsystem. The simulation results indicate the contribution of the LQR controller to the bridge crane's stability [6]. The control strategy proposed by Ngo combines a fuzzy sliding mode control approach with a Kalman filter-based MH roll angle prediction algorithm. In addition to simulation and experimentation, the efficacy of the proposed offshore container crane control system is validated [7]. Qian et al. constructed a novel approach for adaptive robust coupling control that simultaneously suppresses load oscillation and cancels out disturbances. It is rigorously proved that the suggested strategy can guarantee the stability of the entire crane system at the equilibrium point. To construct a dynamic model of a crane system, Kim et al. suggested a robust anti-sway control based on neural networks; the asymptotic stability of the sliding manifold is demonstrated by Lyapunov analysis, and simulation results show the efficacy and resilience of the proposed control method. Although these techniques may forecast and control the payload swing during ship excitation, they cannot remove it entirely and are not generally employed in engineering.

Simultaneously, the mechanical analysis of the maritime crane system and the precision of dynamic models are essential to the investigation of the anti-swing problem [10]. In order to assist the study of this problem through dynamic simulation analysis, much of the research treats the hook and payload as a single system. Aksjonov et al. derived a mathematical model of a three-dimensional crane by using the Euler–Lagrange technique; a 5 degrees of freedom (5DOF) control technique was devised, examined and compared with various load masses. On the basis of dynamic analysis, Sun et al. construct nonlinear dynamic equations for OCC systems exposed to ship motion, then a two-layer sliding manifold is constructed to concurrently provide position tracking and sway control independent of ship motion and parameter disturbances. Huang et al. proposed a combined command shaping and feedback control system. The input shaper removes oscillations in the payload produced by human operator commands, while the feedback controller mitigates the impacts of wind. Miranda-Colorado presented a novel model-free robust control scheme for the attenuation of payload swing angles in two-dimensional crane systems with varying rope lengths. Jensen created the 2-DOF anti-sway controller by deriving the suspension load dynamics and the pertinent kinematics of the crane; an anti-sway controller is added to the electro-hydraulic motion controller via feedforward. The payload mimics a nonlinear pendulum system in this manner. In actuality, a double-pendulum effect will occur when the mass of the payload and the hook are somewhat similar and there is a particular distance between the payload and hook. The nonlinear dynamic model of the double-pendulum crane is more sophisticated than that of the single-pendulum type, as are the degree of nonlinearity and underactuation of the system, the connection between the double-pendulum cranes, and the study on the anti-swing strategy. For instance, in the ship-mounted batch transfer hanging basket, the basket and the hook are connected by a long steel cable, and the swinging motion of the hanging basket and hook will generate a dynamic coupling connection. Once there is an evident swing during the transfer of the hanging basket, the operator can either wait for the swing to cease automatically or actively push and pull the hanging basket to prevent it from swinging. The operating efficiency is low, as is the degree of automation, which might lead to accidents and deaths of deck building workers in adverse sea conditions.

The majority of the study on double-pendulum cranes has been on non-excited bridge cranes; current research on anti-swing jib crane technologies is sparse. For instance, Shi et al. suggested a nonlinear coupled tracking anti-swing controller for gantry cranes and validated the performance of the controller by theoretical derivation, modelling, and testing. Qiang et al. developed a nonlinear dynamic model of a double-pendulum crane and a controller based on the radial basis function (RBF) neural network compensated adaptive approach. The compensator's ability to enhance the controller's control performance is confirmed. Ren et al. suggested a generic model-free anti-swing strategy that does not need consideration of the space state equation and can eliminate payload swing independent of the system design.

Although researchers have studied the plane swing of the double-pendulum bridge crane and other scholars have studied the in-plane and out-of-plane swing of the single-pendulum marine crane under wave excitation [19], there is a dearth of research on the in-plane and out-of-plane anti-swing of the double-pendulum jib cranes under ship excitation. Wang et al. proposed a three-cord traction mechanical anti-swing device and developed its geometric and dynamic models; they presented how to suppress the swing of a single pendulum and a tension-setting method based on the damping principle. Therefore, the primary objective of this article is to develop a precise dynamic model of the in-plane and out-of-plane oscillation of the double pendulum under the coupled circumstances of wave excitation and payload inertia. The second aim of this paper is to suggest a parallel main and auxiliary cable that provides a 2DOF anti-swing control mechanism for traction. The primary and auxiliary traction cables are used to create traction on the payload to prevent the double pendulum from oscillating.

Regarding the arrangement of this work, the structural concept of a 2DOF parallel anti-swing device with main and auxiliary cables is first introduced. Second, a model is developed to describe the payload dynamics of the double-pendulum jib crane under the influence of the ship's rolling and pitching and the operation of the anti-swing mechanism. Matlab/Simulink is used to simulate the dynamics of this model in order to ease the examination of the influence of the anti-swing device under various operating situations, including crane settings. Finally, an experimental validation is conducted to provide credibility to the results stated in this study methodology.

STRUCTURE OF ANTI-SWING DEVICE AND CONTROL SYSTEM PRINCIPLE

In this proposed method, the ship-mounted 2DOF parallel anti-swing device is composed of a hydraulic pump station, a mechanical winch, and a crane control system. Additionally, to maximize the functional features of the crane, a small working space, reasonable structure, high safety and good cooperation is needed. As shown in Fig. 1, a marine crane anti-swing device consists of a crane, a folding arm, and auxiliary cables. Additionally, there are three auxiliary cables, which are controlled by three hydraulic motors respectively. Two of these auxiliary cables are connected to the hook from the top pulley of the folding arm, and the other one to the hook through the pulley of the boom. When the auxiliary cables are all tensioned, the triangular connection point hinders the movement of the hook and indirectly controls the swing of the payload. The purpose of this setup is to achieve the desired anti-swing effect.

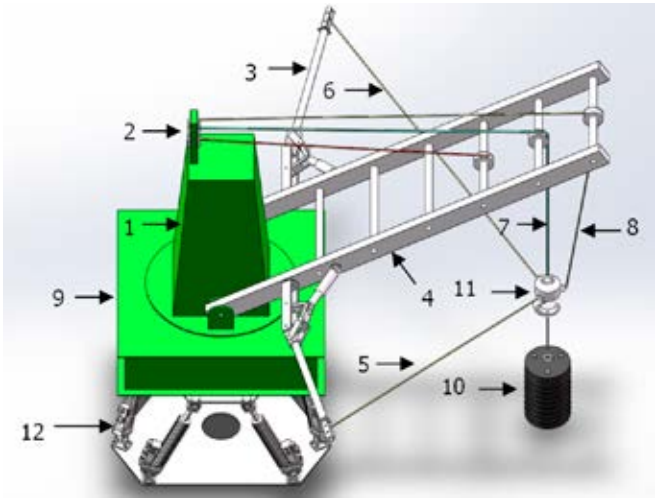

1-Crane body, 2-Pulley set, 3-Folding arm, 4-Crane boom, 5,6,8-Auxiliary cables, 7-Main cable, 9-Crane base, 10-Payload, 11-Hook, 12-6DOF platform

Fig. 1. Double-pendulum anti-swing device for ship-mounted crane

DYNAMICS MODEL AND SIMULATION ANALYSIS OF ANTI-SWING SYSTEM

While the crane's main cables are being retracted and released, the three auxiliary cables also move. The efficient functioning of the crane is ensured by the tight coordination between these cables. To avoid the auxiliary cable sagging and shaking, the force and velocity of the auxiliary cable must fulfil the payload system's static equilibrium parameters. Otherwise, it may not only hinder the payload's swing but also enhance it. In light of this issue, it is required to develop a precise dynamic model of the ship's anti-swing device.

In order to assist the research of the anti-swing issue, the following assumptions were made:

(1) Since the auxiliary cables and main cable are composed of a non-retractable, flexible material, the weight of the cable is insignificant.
(2) The anti-swing does not account for the rotation of the crane, so only the in-plane and out-of-plane angles of the load induced by the rotation of the crane boom are considered.
(3) Because the raising and lowering of the boom has no effect on the anti-swing device, the angle of the boom variation is fixed at a constant value.
(4) The wave excitation transmission to the payload and the impact of the elastic deformation of the ship, crane body, and boom on the excitation transmission are not taken into account.
(5) The hook and the payload are considered to be two spherical objects with identical density and regular forms.

GEOMETRIC MODEL OF ANTI-SWING DEVICE

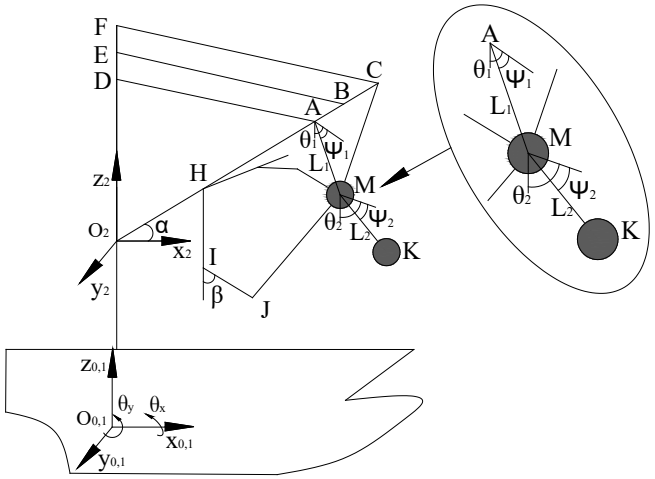

Fig. 2. Schematic diagram of double-pendulum anti-swing device for ship-mounted crane

Fig. 2 shows the schematic diagram of the double-pendulum anti-swing device for a ship-mounted crane. A is the suspension point, the weight of the hook M is m_1, the weight of the payload K is m_2, the length of the connecting rope in the middle is L_2, and the length of the main cable MA is L_1. MC, MJ, and MQ are three auxiliary cables. The boom luffing angle α, the out angle of the auxiliary cable β, the maximum roll angle of the ship φ_x, and the maximum pitch angle of the ship φ_y, are also given in the figure. Given the initial in-plane and out-of-plane angles, and that the hook and payload swing angles in the $o_1 - x_1 z_1$ are θ_1 and θ_2, and in the $o_1 - x_1 y_1$ are ψ_1 and ψ_2 respectively, the following is true in the inertial coordinate system:

$$ {}^{0}P_M = \begin{bmatrix} x_M & y_M & z_M \end{bmatrix}^T = \begin{bmatrix} x_2 & y_2 & z_2 \end{bmatrix}^T = \begin{bmatrix} x_A + L_1 \cos\psi_1 \sin\theta_1 \\ y_A + L_1 \sin\psi_1 \\ z_A - L_1 \cos\psi_1 \cos\theta_1 \end{bmatrix} \quad (1) $$

$$ {}^0P_J = \begin{bmatrix} x_J & y_J & z_J \end{bmatrix}^T = \begin{bmatrix} L_{OH}\cos\alpha + L_{IJ}\sin\beta\cos\alpha \\ -L_{HI} - L_{IJ}\cos\beta \\ L_{OH}\sin\alpha + L_{IJ}\sin\beta\sin\alpha \end{bmatrix} \tag{2} $$

$$ {}^0P_Q = \begin{bmatrix} x_Q & y_Q & z_Q \end{bmatrix}^T = \begin{bmatrix} x_J & -y_J & z_J \end{bmatrix}^T \tag{3} $$

$$ {}^0P_C = \begin{bmatrix} L_{OC}\cos\alpha & 0 & L_{OC}\sin\alpha \end{bmatrix}^T \tag{4} $$

$$ {}^0P_K = \begin{bmatrix} x_3 & y_3 & z_3 \end{bmatrix}^T = \begin{bmatrix} x_A + L_1\cos\psi_1\sin\theta_1 + L_2\cos\psi_2\sin\theta_2 \\ y_A + L_1\sin\psi_1 + L_2\sin\psi_2 \\ z_A - L_1\cos\psi_1\cos\theta_1 - L_2\cos\psi_2\cos\theta_2 \end{bmatrix} \tag{5} $$

Consequently, the lengths of the auxiliary cables MJ and MC are as follows:

$$ L_{MJ} = \sqrt{\begin{aligned} &\left(x_A + L_1\cos\psi_1\sin\theta_1 - L_{OH}\cos\alpha - L_{IJ}\sin\beta\cos\alpha\right)^2 + \\ &\left(y_A + L_1\sin\theta_1 - L_{HI} - L_{IJ}\cos\beta\right)^2 + \\ &\left(z_A - L_1\cos\psi_1\cos\theta_1 - L_{OH}\sin\alpha - L_{IJ}\sin\beta\sin\alpha\right)^2 \end{aligned}} \tag{6} $$

$$ L_{MC} = \sqrt{\begin{aligned} &\left(x_A + L_1\cos\psi_1\sin\theta_1 - L_{OC}\cos\alpha\right)^2 + \left(y_A + L_1\sin\theta_1\right)^2 \\ &+\left(z_A - L_1\cos\psi_1\cos\psi_1 - L_{OC}\sin\alpha\right)^2 \end{aligned}} \tag{7} $$

KINEMATIC MODEL OF THE ANTI-SWING DEVICE

This paper explores the effect of ship roll and pitch excitation on the payload. Defining as R_x, R_y the hull's rotation matrix about the x, y axes, their rotation matrices are [21]:

$$ R_x = \begin{bmatrix} 1 & 0 & 0 \\ 0 & \cos\theta_x & \sin\theta_x \\ 0 & -\sin\theta_x & \cos\theta_x \end{bmatrix} \tag{8} $$

$$ R_y = \begin{bmatrix} \cos\theta_y & 0 & -\sin\theta_y \\ 0 & 1 & 0 \\ \sin\theta_y & 0 & \cos\theta_y \end{bmatrix} \tag{9} $$

Assume that ${}^m_nR$ is the rotation matrix from (x_n, y_n, z_n) to (x_m, y_m, z_m). The transformation matrix of the payload with respect to the dynamic coordinate system is as follows:

$$ {}^0P_A = {}_0^1R^T\,{}^1P_2 + {}_1^2R^T\,{}^2P_A = \begin{bmatrix} x_1 & y_1 & z_1 \end{bmatrix}^T = \begin{bmatrix} \left(L_x + L_{OA}\cos\alpha\right)\cos\theta_y + L_y\sin\theta_x\sin\theta_y - \left(L_z + L_{OA}\cos\alpha\right)\sin\theta_y\cos\theta_x \\ L_y\cos\theta_x + \left(L_z + L_{OA}\cos\alpha\right)\sin\theta_x \\ \left(L_x + L_{OA}\cos\alpha\right)\sin\theta_y - L_y\sin\theta_x\cos\theta_y + \left(L_z + L_{OA}\sin\alpha\right)\cos\theta_x\cos\theta_y \end{bmatrix} \tag{10} $$

(L_x, L_y, L_z) is the position coordinate of the crane base relative to the coordinate system O_0-$x_0y_0z_0$.

DYNAMIC MODEL OF THE HOOK

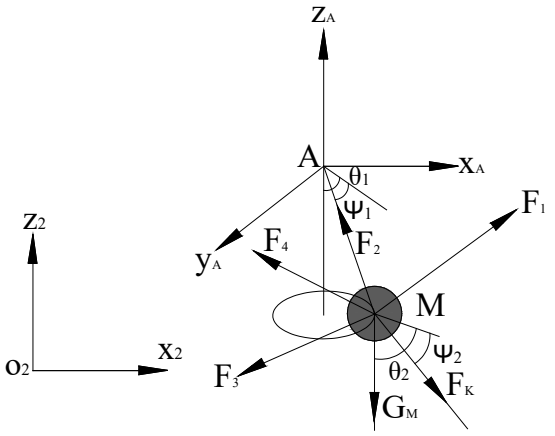

Fig. 3. Stress analysis diagram of hook

Fig. 3 depicts the force on the hook. F_1, F_3, F_4 is the pulling force of the three auxiliary cables on the hook, F_2 is the tension of the main cable on the hook, F_K is the pulling force of the payload on the hook, G_M is the hook weight, and the components of the tension of the three auxiliary cables in the x, y, and z axes are defined as follows:

$$ \begin{cases} F_{ix} = \left|F_i\right| i_{ix} \\ F_{iy} = \left|F_i\right| i_{iy}, (i = 1,2,3) \\ F_{iz} = \left|F_i\right| i_{iz} \end{cases} \tag{11} $$

where

$$ i_{1x} = \frac{x_C - x_M}{L_{MC}}, i_{1y} = \frac{y_C - y_M}{L_{MC}}, i_{1z} = \frac{z_C - z_M}{L_{MC}}, i_{3x} = \frac{x_Q - x_M}{L_{MQ}}, i_{3y} = \frac{y_Q - y_M}{L_{MQ}}, $$
$$ i_{3z} = \frac{z_Q - z_M}{L_{MQ}}, i_{4x} = \frac{x_J - x_M}{L_{MJ}}, i_{4y} = \frac{y_J - y_M}{L_{MJ}}, i_{4z} = \frac{z_J - z_M}{L_{MJ}}. $$

According to Newton's second law, the equation of motion for the hook along the coordinate axes *x*, *y*, and *z* is derived as follows:

$$ \begin{cases} m_1\ddot{x}_2 = F_{1x} - F_{3x} - F_{4x} - F_{2x} + F_{Kx} \\ m_1\ddot{y}_2 = -F_{1y} + F_{3y} - F_{4y} - F_{2y} + F_{Ky} \\ m_1\ddot{z}_2 = F_{1z} - F_{3z} - F_{4z} + F_{2z} - F_{Kz} - m_1 g \end{cases} \tag{12} $$

where $\ddot{x}_2, \ddot{y}_2, \ddot{z}_2$ are the acceleration of the hook in the x, y, z directions,

$$ \begin{cases} F_{Kx} = (m_2 g\cos\theta_2\cos\psi_2 + \frac{1}{2}m_2\left(\frac{\ddot{\psi}_2\sin\psi_2\cos\theta_2 + \dot{\theta}_2\sin\theta_2\cos\psi_2}{\sqrt{1-\cos\psi_2\cos\theta_2}}\right)^2 L_2)\cos\psi_2\sin\theta_2 \\ F_{Ky} = (m_2 g\cos\theta_2\cos\psi_2 + \frac{1}{2}m_2\left(\frac{\ddot{\psi}_2\sin\psi_2\cos\theta_2 + \dot{\theta}_2\sin\theta_2\cos\psi_2}{\sqrt{1-\cos\psi_2\cos\theta_2}}\right)^2 L_2)\sin\psi_2 \\ F_{Kz} = (m_2 g\cos\theta_2\cos\psi_2 + \frac{1}{2}m_2\left(\frac{\ddot{\psi}_2\sin\psi_2\cos\theta_2 + \dot{\theta}_2\sin\theta_2\cos\psi_2}{\sqrt{1-\cos\psi_2\cos\theta_2}}\right)^2 L_2)\cos\psi_2\cos\theta_2 \end{cases} $$

From Equation (1), the following equations are given as follows:

$$\begin{cases} \ddot{x}_2 = \ddot{x}_1 + L_1\cos\theta_1\left(\ddot{\theta}_1\cos\psi_1 - 2\dot{\theta}_1\dot{\psi}_1\sin\psi_1\right) - \\ \qquad L_1\sin\theta_1\left(\cos\psi_1\left(\dot{\theta}_1^2+\dot{\psi}_1^2\right)+\ddot{\psi}_1\sin\psi_1\right) \\ \ddot{y}_2 = \ddot{y}_1 + L_1\ddot{\psi}_1\cos\psi_1 - L_1\dot{\psi}_1^2\sin\psi_1 \\ \ddot{z}_2 = \ddot{z}_1 + L_1\begin{pmatrix}\cos\theta_1\cos\psi_1\left(\dot{\theta}_1^2+\dot{\psi}_1^2\right) - 2\dot{\theta}_1\dot{\psi}_1\sin\theta_1\sin\psi_1 + \\ \ddot{\theta}_1\sin\theta_1\cos\psi_1 + \ddot{\psi}_1\cos\theta_1\sin\psi_1\end{pmatrix} \end{cases} \tag{13}$$

where $\ddot{x}_1, \ddot{y}_1, \ddot{z}_1$ can be obtained from Equation (10).

Postulating that $f_x = F_{1x} - F_{3x} - F_{4x}$ $f_y = -F_{1y} + F_{3y} - F_{4y}$ $f_z = F_{1z} - F_{3z} - F_{4z}$ and applying it to (12), the result is represented as:

$$\begin{cases} m_1\ddot{x}_2 = f_x + F_{Kx} - \left|F_2\right|\cos\psi_1\sin\theta_1 \\ m_1\ddot{y}_2 = f_y + F_{Ky} - \left|F_2\right|\sin\psi_1 \\ m_1\ddot{z}_2 = f_z - F_{Kz} + \left|F_2\right|\cos\psi_1\cos\theta_1 - m_1 g \end{cases} \tag{14}$$

By eliminating $\left|F_2\right|$ from Equation (14), the results can be given as follows:

$$\begin{cases} \tan\psi_1\left(f_x + F_{Kx} - m_1\ddot{x}_2\right) = \sin\theta_1\left(f_y + F_{Ky} - m_1\ddot{y}_2\right) \\ \tan\theta_1\left(-f_z + F_{Kz} + m_1\ddot{z}_2 + m_1 g\right) = \cos\theta_1\left(f_y + F_{Ky} - m_1\ddot{y}_2\right) \end{cases} \tag{15}$$

Applying Equations (11) and (13) into (15) yields:

$$\ddot{\theta}_1 = \frac{\begin{array}{l}\sin\theta_1\left(\begin{array}{l}\cos\theta_1\left(f_y + F_{Ky} - m_1\left(\ddot{y}_1 - L_1\dot{\psi}_1^2\sin\psi_1\right)\right) - \tan\psi_1 \\ \left(-f_z + F_{Kz} + m_1 g + m_1\begin{pmatrix}\ddot{z}_1 + L_1\cos\theta_1\cos\psi_1\left(\dot{\theta}_1^2+\dot{\psi}_1^2\right) \\ -2L_1\dot{\theta}_1\dot{\psi}_1\sin\theta_1\sin\psi_1\end{pmatrix}\right)\end{array}\right) \\ -\cos\theta_1\left(\begin{array}{l}\sin\theta_1\left(f_y + F_{Ky} - m_1\left(\ddot{y}_1 - L_1\dot{\psi}_1^2\sin\psi_1\right)\right) \\ -\tan\psi_1\left(f_x + F_{Kx} - m_1\begin{pmatrix}\ddot{x}_1 - 2L_1\dot{\theta}_1\dot{\psi}_1\cos\theta_1\sin\psi_1 - \\ L_1\sin\theta_1\cos\psi_1\left(\dot{\theta}_1^2+\dot{\psi}_1^2\right)\end{pmatrix}\right)\end{array}\right)\end{array}}{m_1 L_1\sin\psi_1} \tag{16}$$

$$\ddot{\psi}_1 = \frac{\begin{array}{l}\sin\theta_1\left(\begin{array}{l}\sin\theta_1\left(f_y + F_{Ky} - m_1\left(\ddot{y}_1 - L_1\dot{\psi}_1^2\sin\psi_1\right)\right) - \tan\psi_1 \\ \left(f_x + F_{Kx} - m_1\left(\ddot{x}_1 - 2L_1\dot{\theta}_1\dot{\psi}_1\cos\theta_1\sin\psi_1 - L_1\sin\theta_1\cos\psi_1\left(\dot{\theta}_1^2+\dot{\psi}_1^2\right)\right)\right)\end{array}\right) \\ +\cos\theta_1\left(\begin{array}{l}\cos\theta_1\left(f_y + F_{Ky} - m_1\left(\ddot{y}_1 - L_1\dot{\psi}_1^2\sin\psi_1\right)\right) \\ -\tan\psi_1\left(-f_z + F_{Kz} + m_1 g + m_1\begin{pmatrix}\ddot{z}_1 + L_1\cos\theta_1\cos\psi_1\left(\dot{\theta}_1^2+\dot{\psi}_1^2\right) \\ -2L_1\dot{\theta}_1\dot{\psi}_1\sin\theta_1\sin\psi_1\end{pmatrix}\right)\end{array}\right)\end{array}}{m_1 L_1\left(\cos\psi_1 + \sin\psi_1\tan\psi_1\right)} \tag{17}$$

DYNAMIC MODEL OF THE PAYLOAD

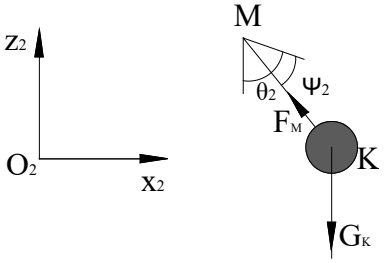

Fig. 4. Stress analysis diagram of payload

The payload K is exposed to the combined effects of gravity G_K and tension F_K to generate a pendulum motion. According to Newton's second law, the equation of motion in the x, y, and z directions is derived as follows:

$$\begin{cases} m_2\ddot{x}_3 = -\left|F_K\right|\cos\psi_2\sin\theta_2 \\ m_2\ddot{y}_3 = -\left|F_K\right|\sin\psi_2 \\ m_2\ddot{z}_3 = \left|F_K\right|\cos\psi_2\cos\theta_2 - m_2 g \end{cases} \tag{18}$$

With Equation (5), the accelerations of the payload can be obtained as follows:

$$\begin{cases} \ddot{x}_3 = \ddot{x}_2 + L_2\cos\theta_2\left(\ddot{\theta}_2\cos\psi_2 - 2\dot{\theta}_2\dot{\psi}_2\sin\psi_2\right) - \\ \qquad L_2\sin\theta_2\left(\cos\psi_2\left(\dot{\theta}_2^2+\dot{\psi}_2^2\right)+\ddot{\psi}_2\sin\psi_2\right) \\ \ddot{y}_3 = \ddot{y}_2 + L_2\ddot{\psi}_2\cos\psi_2 - L_2\dot{\psi}_2^2\sin\psi_2 \\ \ddot{z}_3 = \ddot{z}_2 + L_2\begin{pmatrix}\cos\theta_2\cos\psi_2\left(\dot{\theta}_2^2+\dot{\psi}_2^2\right) - 2\dot{\theta}_2\dot{\psi}_2\sin\theta_2\sin\psi_2 \\ +\ddot{\theta}_2\sin\theta_2\cos\psi_2 + \ddot{\psi}_2\cos\theta_2\sin\psi_2\end{pmatrix} \end{cases} \tag{19}$$

Substituting (19) into (18) and eliminating F_K leads to:

$$\ddot{\theta}_2 = \frac{\begin{array}{l}\cos\theta_2\left(\sin\theta_2\left(\ddot{y}_2 - L_2\dot{\psi}_2^2\sin\psi_2\right) - \tan\psi_2\left(\begin{array}{l}\ddot{x}_2 - 2L_2\dot{\theta}_2\dot{\psi}_2\cos\theta_2\sin\psi_2 - \\ L_2\sin\theta_2\cos\psi_2\left(\dot{\psi}_2^2+\dot{\theta}_2^2\right)\end{array}\right)\right) - \\ \sin\theta_2\left(\cos\theta_2\left(\ddot{y}_2 - L_2\dot{\psi}_2^2\sin\psi_2\right) + \tan\psi_2\left(\begin{array}{l}\ddot{z}_2 + g + \\ L_2\begin{pmatrix}\cos\psi_2\cos\theta_2\left(\dot{\psi}_2^2+\dot{\theta}_2^2\right) \\ -2\dot{\theta}_2\dot{\psi}_2\sin\theta_2\sin\psi_2\end{pmatrix}\end{array}\right)\right)\end{array}}{L_2\sin\psi_2} \tag{20}$$

$$\ddot{\psi}_2 = -\frac{\begin{array}{l}\cos\theta_2\left(\begin{array}{l}\cos\theta_2\left(\ddot{y}_2 - L_2\dot{\psi}_2^2\sin\psi_2\right) + \\ \tan\psi_2\left(\ddot{z}_2 + g + L_2\left(\cos\psi_2\cos\theta_2\left(\dot{\psi}_2^2+\dot{\theta}_2^2\right) - 2\dot{\theta}_2\dot{\psi}_2\sin\theta_2\sin\psi_2\right)\right)\end{array}\right) + \\ \sin\theta_2\left(\begin{array}{l}\sin\theta_2\left(\ddot{y}_2 - L_2\dot{\psi}_2^2\sin\psi_2\right) - \\ \tan\psi_2\left(\ddot{x}_2 - 2L_2\dot{\theta}_2\dot{\psi}_2\cos\theta_2\sin\psi_2 - L_2\sin\theta_2\cos\psi_2\left(\dot{\psi}_2^2+\dot{\theta}_2^2\right)\right)\end{array}\right)\end{array}}{L_2\left(\sin\psi_2\tan\psi_2 + \cos\psi_2\right)} \tag{21}$$

AUXILIARY CABLE TENSION CONTROL

The main cable must maintain a steady tension while raising the payload. If the cable becomes slack, retightening it will result in a sling vibration or possibly cause it to break. In addition, once the main cable is released, the auxiliary cables will bear the weight of the payload. Such circumstance will dramatically stress the auxiliary cables and overload the traction motor, causing the whole system to fall out of balance. Consequently, the tension set of the auxiliary cables must satisfy the following:

$$\begin{cases} if \ \ \dot{\psi}_1 \geqslant 0 & |F_3| = F_3 \ \ |F_4| = K_l G_M |\dot{\psi}_1| \\ if \ \ \dot{\psi}_1 < 0 & |F_4| = F_4 \ \ |F_3| = K_l G_M |\dot{\psi}_1| \\ if \ \ \dot{\theta}_1 \geqslant 0 & |F_1| = 0 \\ if \ \ \dot{\theta}_1 < 0 & |F_1| = K_1 G_M |\dot{\theta}_1| \end{cases} \tag{22}$$

where K is the tension coefficient and F_i (i=1,2,3) is the auxiliary cable tension set.

Air resistance and rope friction are responsible for the swing of the payload. The direction of the combined force will always be perpendicular to the direction of motion, which eventually causes the swinging of the payload to cease. Despite being a typical phenomenon, it is impossible to forecast when this process will occur. Given the above premise, a technique for controlling the tension of the auxiliary cables is provided to ensure that each auxiliary cable is capable of preventing the payload from swinging. The tension setting for the auxiliary cable must comply with the following relationship:

$$\begin{cases} F_1 - \delta_1 \leqslant |F_1| & F_1 + \delta_1 \\ F_3 - \delta_3 \leqslant |F_3| & F_3 + \delta_3 \\ F_4 - \delta_4 \leqslant |F_4| & F_4 + \delta_4 \end{cases} \tag{23}$$

where δ_i (i=1,2,3) is the threshold value for auxiliary cable tension.

DYNAMIC SIMULATION ANALYSIS

To verify the dynamic characteristics of the model, combined with the laboratory crane model shown in Fig. 2, the system parameters are set as follows:

$m_1 = 5kg, m_2 = 10kg, L_{OC} = 1.7m, L_{HI} = 0.25m,$

$L_{HM} = 1.7m, L_{IJ} = 0.75m, L_{O_1H} = 0.32m,$

$L_{O_2A} = 1.2m, L_{AM} = 1.5m, \alpha = 10°, \beta = 45°, K = 0.8$.

The simulation analysis for the in-plane and out-plane angles of the double pendulum may be done based on Equations (18), (19) and (22).

SIMULATION ANALYSIS OF DOUBLE-PENDULUM DYNAMIC WITHOUT SHIP EXCITATION

In the absence of ship excitation, the emphasis of the study was on the effect of the double-pendulum swing law and double-pendulum spacing. On the impact of the anti-swing, the length of the main cable and damping coefficient were also taken into account.

The swing law of double pendulum without anti-swing device

Let the weight of the double pendulum be m_1=5kg, m_2=10kg, respectively; the in-plane swing angle of the first-level pendulum is θ_1=20°, and the in-plane swing angle of the second-level pendulum is θ_2=20°. Fig. 5 illustrates the swing of the double pendulum. Fig. (a) depicts the oscillogram of the primary-pendulum swing while the double pendulum is shown swinging periodically. Curve A is the swing of the primary pendulum without interference, and curve B is the swing of the primary pendulum with secondary-pendulum interference; the initial angle of the hook is 10°, whereas the maximum swing angle is close to 14°. The angle of the swing increases while the primary-pendulum swing is affected by the secondary pendulum. In Fig. (b), curve C is the swing of the secondary pendulum without interference, and curve D is the swing of the secondary pendulum with primary-pendulum interference. The oscillogram of the secondary-pendulum swing reveals that the angle of the payload begins at 20°, while the maximum value of the swing cycle is close to 15°. It can also be seen that as the angle of the secondary pendulum is being affected by the primary pendulum the swing angle decreases.

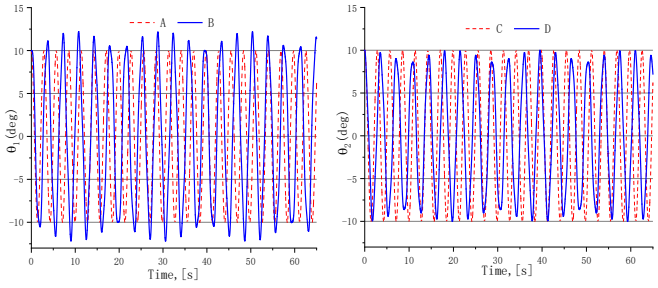

(a) Primary-pendulum swing *(b) Secondary-pendulum swing*

Fig. 5. Double-pendulum swing oscillogram

Effects of the main cable length on the double pendulum

The length of the main cable is modelled as 1 m, 3 m, 5 m, 7 m and 9 m respectively to examine how the length of the cable affects the double-pendulum swing. Fig. 6 (a) illustrates the swing principle on the primary-pendulum swing with the different cable lengths. Fig. 6 (b) shows a regular sinusoidal motion of the swing principle of the secondary-pendulum payload. Additionally, the comparison demonstrates that the longer the main cable, the greater the swing period of the double pendulum and the smaller the swing frequency. With the increased length of the main cable, the maximum

value of the secondary pendulum's period approaches the original angle. The same effect, however, cannot be observed in the primary pendulum.

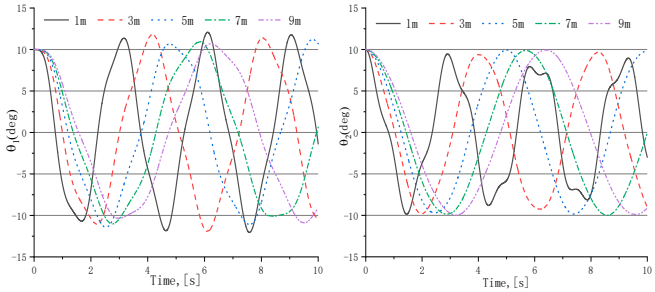

(a) Primary-pendulum swing *(b) Secondary-pendulum swing*

Fig. 6. Double-pendulum swing in-plane oscillogram

Influence of control cable force on in-plane swing

The coefficient K_l of the anti-swing device is modelled using the values 0.05, 0.1, and 0.15, which are given in Equation (22). Fig. 7 illustrates the impact of the control cable force on the in-plane swing. Fig. 7 (a) shows the in-plane angles of the primary pendulum, whereas Fig. 7 (b) depicts the in-plane angles of the secondary pendulum. The stabilization time of the double pendulum under distinct coefficients is 25 s, 35 s, and 65 s accordingly. The diagrams reveal that the stability time of the payload system reduced as the force increased, whereas the stabilization time of the double pendulum remained constant.

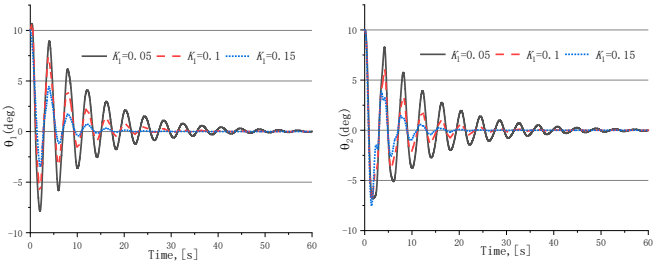

(a) Primary-pendulum swing *(b) Secondary-pendulum swing*

Fig. 7. In-plane angle of double pendulum under different weights

SIMULATION ANALYSIS OF DOUBLE-PENDULUM DYNAMICS UNDER SHIP EXCITATION

Effects of ship's rolling and pitching on double pendulum

The initial in-plane and out-of-plane swing angles of the double pendulum are both 10°, the main cable is L_1, the double-pendulum swing characteristic frequency is ω_n and calculated by Equation (24), while the ship's rolling and pitching excitation frequencies are $0.6\omega_n$, $0.8\omega_n$, ω_n, $1.2\omega_n$ respectively. Fig. 8 shows the double-pendulum swing. Resonance occurred if the excitation frequency of the ship was proportional to the frequency of the anti-swing system. Consequently, the double pendulum swung vigorously until its swing amplitude surpassed the maximum amount of 30°. In contrast, when the simulation frequency is not proportional to the ship's rolling frequency, the swing amplitude of the payload tends to increase and then subsequently decrease.

The characteristic frequency of the anti-swing device is:

$$\omega_n = 1/2\pi\sqrt{l/g} \tag{24}$$

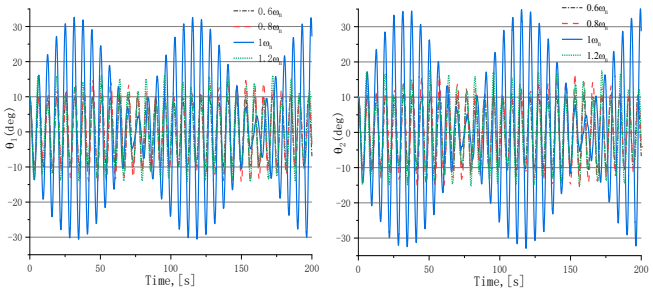

(a) Primary-pendulum swing (b) Secondary-pendulum swing

Fig. 8. Double-pendulum swing oscillogram

Effects of ship excitation on the anti-swing device

Table 1 displays the ship motion parameters under different sea states as the ship is subjected to the coupled effect of rolling and pitching.

Tab. 1. Ship motion parameters under different sea states

International sea scale	Rolling amplitude (deg)	Pitching amplitude (deg)	Rolling period (s)	Pitching period (s)
4 sea state	5	1	14.8	6
5 sea state	9	2	14.8	6
6 sea state	13	3	14.8	6

The traction coefficient of the auxiliary cables is assumed to be 0.05, and the initial in-plane and out-of-plane swing angles are both 10°. The suppressing impact of the double-pendulum anti-swing device under distinct sea conditions is shown in Fig. 9. Under the influence of the double-pendulum anti-swing device, the in-plane and out-of-plane angles of the double pendulum are rapidly and considerably attenuated. Fig. (a) represents the in-plane angle swing curve of the primary pendulums, in which it can be observed that the angle is reduced from 10° to around 1°, or by 90%. Fig. (b) depicts the out-of-plane angle swing curve, where the angle is reduced by 80% from 10° to around 2°. Fig. (c) demonstrates the in-plane angle swing curve of the secondary pendulums, in which the angle is reduced by 90% from 10° to about 1°. The angle depicted on the out-of-plane angle swing curve in Fig. (d) is decreased by 80%, from 10° to around 2°. From the swing curves of the in-plane and out-of-plane angles of the double pendulum, it can be determined that the double-pendulum anti-swing technique presented in this paper has a greater effect on the in-plane swing than the out-of-plane swing for the double pendulum, and that the worse the sea conditions are, the less effective the swing suppression effect.

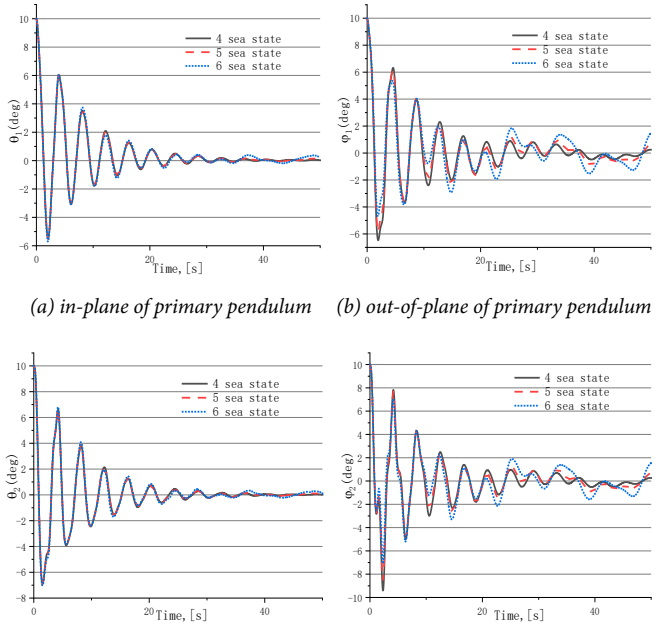

(a) in-plane of primary pendulum (b) out-of-plane of primary pendulum

(c) in-plane of secondary pendulum (d) out-of-plane of secondary pendulum

Fig. 9. Double-pendulum swing oscillogram

TEST COMPARISON AND VERIFICATION

To validate the dynamic model and simulation, an anti-swing test platform based on the double-pendulum anti-swing device for ship-mounted jib cranes, as illustrated in Fig. 10, is constructed. The platform testing data parameters were $m_1 = 20kg$ and $m_2 = 20kg$. The length of the main cable is 1 m, while the length of the connecting cable between the two pendulums is 0.5 m. Furthermore, the initial swing angles of the double pendulum in-plane and out-of-plane were both modelled at a 10° angle, and data samples are acquired every 0.03s throughout each swing.

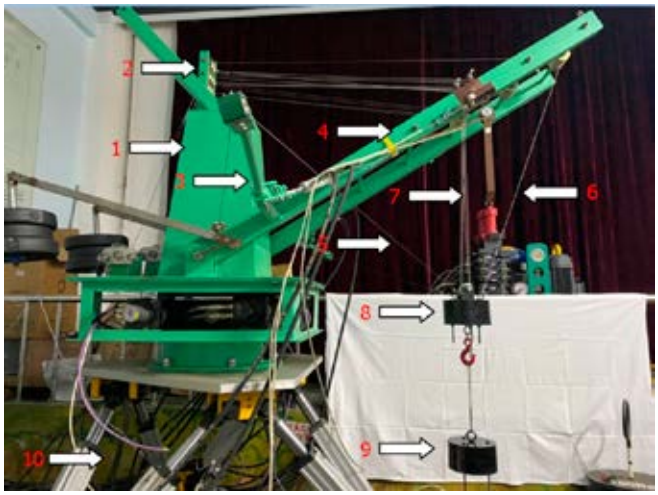

1 - Crane body, 2 - Pulley set, 3 - Folding arm, 4 - Crane boom, 5,6 -Auxiliary cables, 7 - Main cable, 8 - Primary pendulum, 9 - Secondary pendulum, 10 - 6DOF platform

Fig. 10. Experimental setup of payload system

DOUBLE-PENDULUM SWING EXPERIMENT WITHOUT EXCITATION AND ANTI-SWING DEVICE

Fig. 11 depicts the comparison and validation of the dynamic simulation and the experimental value of the in-plane and out-of-plane swing. Fig. 11 (a) represents the in-plane swing curve of the primary pendulum, Fig. 11 (b) shows the in-plane swing curve of the secondary pendulum, Fig. 11 (c) indicates the out-of-plane swing curve of the primary pendulum, and Fig. 11 (d) reflects the out-of-plane swing curve of the secondary pendulum. The comparative study reveals that the theoretical calculation value is compatible with the experimental value, even under varying circumstances. The data demonstrate that the dynamic model of the double-pendulum anti-swing device for ship-mounted jib cranes presented in this paper is accurate. While a high-frequency camera was utilized to capture the swing angles of the double pendulum during the test, there is a degree of discrepancy between the acquired data values and the theoretical values. The mistake is particularly noticeable during image acquisition and processing.

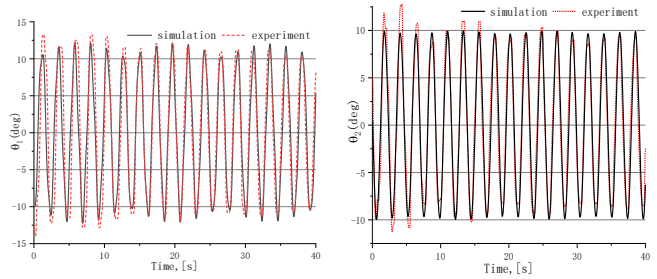

(a) in-plane of primary pendulum (b) out-of-plane of primary pendulum

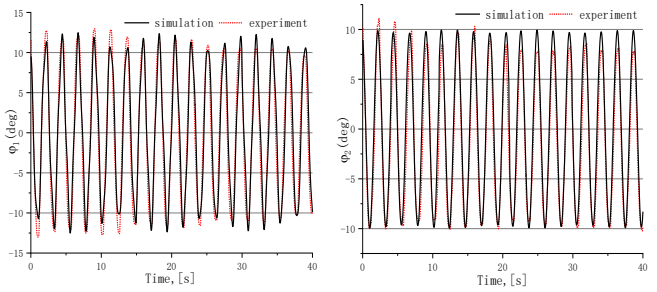

(c) in-plane of secondary pendulum (d) out-of-plane of secondary pendulum

Fig. 11. Double-pendulum swing simulation and experimental comparison

DOUBLE-PENDULUM ANTI-SWING EXPERIMENT UNDER EXCITATION CONDITION

The coefficient of traction of the auxiliary cables is assumed to be 0.5, and a six- degrees-of-freedom platform simulates the sea state of level 5. Fig. 12 compares the dynamic simulation and the experimental data for the in-plane and out-of-plane swings of the double pendulum. The results of the simulation were identical to the experimental data, demonstrating the validity of the present dynamic simulation model. Under

the influence of the double-pendulum anti-swing device, the swing diminished gradually. The decay period is around 4s, while there is a continuous swinging. There is still a periodic 2° angle swing despite the fact that the angle of swing has been significantly decreased. This demonstrates that the periodic movement of the sea influences the motion principle of the double pendulum after equilibrium. The in-plane swing angle of the double pendulum is less than the out-of-plane swing angle after the pendulum has attained equilibrium. This suggests that the double pendulum's anti-swing device is more effective on the in-plane swing than the out-of-plane swing.

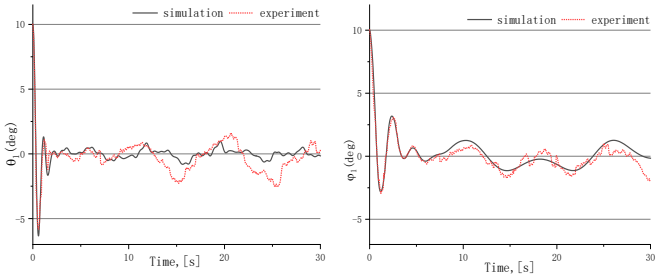

(a) in-plane of primary pendulum (b) out-of-plane of primary pendulum

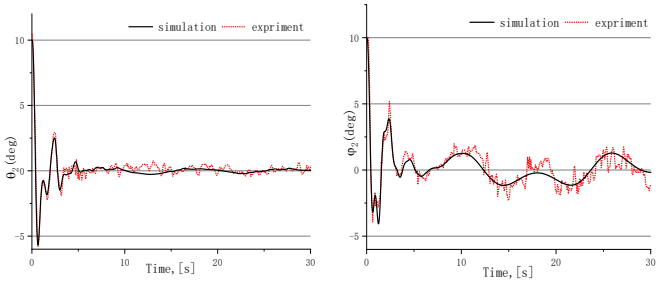

(a) in-plane of secondary pendulum (b) out-of-plane of secondary pendulum

Fig. 12. Double-pendulum anti-swing simulation and experimental comparison

CONCLUSION

The purpose of this paper is to offer a model consisting of a parallel 2DOF anti-swing control approach for underactuated double-pendulum maritime jib cranes that reduces swing. The device's anti-swing mechanism is investigated, and a precise dynamic model of the double pendulum is given. The impacts of ship excitation, the main cable length, second-level pendulum spacing, and auxiliary cable tension on the double-pendulum angle were investigated in detail, and the simulation findings were ultimately verified by the data analysis. Through theoretical research and experimental validation, the following are the main findings of this paper:

(1) Under the impact of ship excitation, the swings of the double-pendulum payload interact, causing the swing of the first-level pendulum to grow and the swing of the second-level pendulum to decrease. The interaction between the two pendulums becomes increasingly apparent as the distance between them decreases.
(2) The dynamic study indicates that raising the tension of the auxiliary cable may improve the suppression impact of the anti-swing device on the double-pendulum payload's oscillation. The primary pendulum decreases the in-plane angle by 90% and the out-of-plane angle by 80%. The in-plane angle of the secondary pendulum is decreased by 90%, while the out-of-plane angle is reduced by 80%, so the pendulum reduction effect is discernible.
(3) The validity of the simulation model and the findings of the dynamics model are validated by comparing and evaluating the experimental and simulation data.

Due to the paucity of research on modelling and finding solutions for double-pendulum anti-swing maritime jib cranes, this paper's accurate dynamic model and experimental methodologies are of great use. In addition, the data and modelling reported in this research may offer more insights for the development of solutions and new modelling concepts applicable to different types of cranes, comparable to the studies on pendulum reduction.

ACKNOWLEDGMENTS

This paper was funded by the National Key Research and Development Program of China (2018YFC0309003), supported by LiaoNing Revitalization Talents Program (XLYC2008018).

DISCLOSURE STATEMENT

There were no possible conflicts of interest revealed by the authors.

REFERENCES

1. E. M. Abdel-Rahman, A. H. Nayfeh, Z. N. Masoud, "Dynamics and control of cranes: A review," *Journal of Vibration and Control*, vol. 9, no. (7), pp. 863–908, 2003, doi:10.1177/1077546303009007007.

2. Chuanzhi Zhu, Guoping Miu, *Theory of ships motion on waves*. Shanghai: Shanghai Jiaotong University Press, 2019.

3. Shenghai Wang, Zhaopeng Ren, Guoliang Jin, Haiquan Chen, "Modeling and Analysis of Offshore Crane Retrofitted with Cable-Driven Inverted Tetrahedron Mechanism," *IEEE Access,* vol. 9, pp. 86132–86143, 2021, doi:

4. 10.1109/ACCESS.2021.3063792.

5. W. Z. Schulz, M. Musatow, C. Jiang, et al., Skin-to-skin replenishment. *Proceedings of the ASNE Symposium on Expeditionary Force Projection*, 2008.

6. M. I. Solihin, A. Legowo, R. Akmeliawati, et al., Robust PID anti-swing control of automatic gantry crane based on Kharitonov's stability. In: *2009 4th IEEE Conference on*

Industrial Electronics and Applications. IEEE, pp. 275–280, 2009.

7. M. Adeli, H. Zarabadipour, S. H. Zarabadi, M. A. Shoorehdeli, Anti-swing control for a double-pendulum-type overhead crane via parallel distributed fuzzy LQR controller combined with genetic fuzzy rule set selection. In: *2011 IEEE International Conference on Control System, Computing and Engineering.* IEEE, pp. 306–311, 2011.

8. Q. H. Ngo, N. P. Nguyen, C. N. Nguyen, T. H. Tran, Q. P. Ha, "Fuzzy sliding mode control of an offshore container crane," *Ocean Eng.*, vol. 140, pp. 125–134, 2017, doi: 10.1016/j.oceaneng.2017.05.019.

9. Y. Qian, Y. Fang, B. Lu, "Adaptive robust tracking control for an offshore ship-mounted crane subject to unmatched sea wave disturbances," *Mech. Syst. Signal Process.*, vol. 114, pp. 556–570, 2018, doi:10.1016/j.ymssp.2018.05.009.

10. G.-H. Kim, P.-T. Pham, Q. H. Ngo, Q. C. Nguyen, "Neural network-based robust anti-sway control of an industrial crane subjected to hoisting dynamics and uncertain hydrodynamic forces," *Int. J. Control Autom. Syst.*, vol. 19, pp. 1953–1961, 2021, doi:10.1007/s12555-020-0333-9.

11. R. Buczkowski and B. Żyliński, "Finite element fatigue analysis of unsupported crane," Polish Marit. Res., vol. 28, no. 1, 2021, doi: 10.2478/pomr-2021-0012.

12. A. Aksjonov, V. Vodovozov, and E. Pellenkov, "Three-dimensional crane modelling and control using Euler-Lagrange state-space approach and anti-swing fuzzy logic," *Electr., Control Commun. Eng.*, vol. 9, no. 1, pp. 5–13, Dec. 2015, doi: 10.1515/ecce-2015-0006.

13. Y. G. Sun, H. Y. Qiang, J. Q. Xu, and D. S. Dong, "The nonlinear dynamics and anti-sway tracking control for offshore container crane on a mobile harbor," *J. Mar. Sci. Technol. - Taiwan, Process.*, vol. 25, no. 6, pp. 656–665, 2017, doi:10.6119/JMST-017-1226-05.

14. J. Huang, E. Maleki, W. Singhose, "Dynamics and swing control of mobile boom cranes subject to wind disturbances," *IET Control Theory and Applications*, vol. 7, no. 9, pp. 1187–1195, 2013, doi:10.1049/iet-cta.2012.0957.

15. R. Miranda-Colorado, "Robust observer-based anti-swing control of 2D-crane systems with load hoisting-lowering," *Nonlinear Dynamics,* vol. 104, no. 4, pp.1–16*r*, 2021, doi:10.1007/s11071-021-06443-x.

16. K. J. Jensen, M. K. Ebbesen, M. R. Hansen, "Anti-swing control of a hydraulic loader crane with a hanging load," *Mechatronics,* vol. 77, 2021, doi: 10.1016/j.mechatronics. 2021. 102599.

17. H. T. Shi, J. Q. Huang, X. Bai, X. Huang, J. Sun, "Nonlinear Anti-swing Control of Underactuated Tower Crane Based on Improved Energy Function," *Int. J. Control Autom. Syst.,* vol. 19, pp. 3967–3982, 2021, doi:10.1007/s12555-020-0292-1.

18. H. Y. Qiang, Y. G. Sun, J. C. Lyu, D. S. Dong, "Anti-Sway and Positioning Adaptive Control of a Double-Pendulum Effect Crane System with Neural Network Compensation," *Front. Robot. AI*, vol. 8, 2021, doi:10.3389/frobt.2021.639734.

19. Zhengru Ren, A. S. Verma, B. Ataei, K. H. Halse, H. P. Hildre, "Model-free anti-swing control of complex-shaped payload with offshore floating cranes and a large number of lift wires," *Ocean Engineering*, vol. 228, pp. 1–13, 2021, doi:10.1016/j.oceaneng.2021.108868.

20. Haiquan Chen, Guoliang Jin, Yang Ji, Anqi Niu, Shenghai Wang, Yuqing Sun, "Simulation and experimental research on constant tension control of traction cable-type anti-swing device for ship-mounted cranes," *Shipbuilding of China*, vol. 62, no. 2, pp. 211–223, 2021.

21. Shenghai Wang, Junjie Wu, Haiquan Chen, Yang Ji, Yuqing Sun, "Dynamic analysis and experiment of the mechanical anti-swing device for ship-mounted cranes," *Journal of Harbin Engineering University*, vol. 40, no. 11, pp. 1858-1864, 2019.

22. J. Ginsberg, *Engineering Dynamics*. New York, NY, USA: *Cambridge Univ. Press*, pp. 99–157, 2008.

23. L. J. Love, J. F. Jansen, F. G. Pin, Compensation of Wave-Induced Motion and Force Phenomena for Ship-Based High Performance Robotic and Human Amplifying Systems, UNT Digital Laboratory, 2003, doi:10.2172/885873.

CONTACT WITH THE AUTHORS

WANG Jianli
e-mail: wangjianli_bohai@126.com

College of Marine Engineering
Dalian Maritime University
Dalian, 116026
China